Dhaka Univ. J. Sci. 73(2): 135-142, 2025 (July)
ISSN 1022 - 2502, E-ISSN 2408-8528
DOI: https://doi.org/10.3329.dujs.v73i2.82772

# Supported Ionic Liquid Phase Materials from 1,8-diazabicyclo[5.4.0]undec-7-ene Based Protic Ionic Liquid and g-$C_3N_4$ and $TiO_2$ Nanoparticles: Preparation and Characterization

**Gulshan Ara[1,2] and Md. Abu Bin Hasan Susan[1*]**

[1]*Department of Chemistry, Faculty of Science, University of Dhaka, Dhaka 1000, Bangladesh*
[2]*Department of Chemistry, Faculty of Science, Jagannath University, Dhaka 1100, Bangladesh*

(Received: 13 April 2025; Accepted: 17 May 2025)

**Abstract**

Supported ionic liquid phase (SILP) materials are a novel approach that blend the benefits of heterogeneous support materials and ionic liquids (ILs) by immobilizing an IL film on a solid phase. In an attempt to modify the surface characteristics of nanoparticles, this study explores a simple refluxing method to prepare two novel SILP materials using two supports, graphitic carbon nitride (g-$C_3N_4$) and titanium dioxide ($TiO_2$) and a 1,8-diazabicyclo[5.4.0]undec-7-ene (DBU) based protic ionic liquid (PIL), 1,8-diazabicyclo[5.4.0]undec-7-ene-8-ium hydroxide ([HDBU]OH). FTIR spectra showed peaks for N-H stretching mode in the region of 3051-3200 $cm^{-1}$ indicating the presence of the PIL in g-$C_3N_4$-[HDBU]OH and $TiO_2$-[HDBU]OH. The distinctly different UV-visible absorption spectra as reflected in absorption maxima in SILP materials compared to the PIL, [HDBU]OH indicates the formation of new materials. The surface morphology and the size of the particles of the SILP materials were determined from SEM images and DLS measurements. The g-$C_3N_4$ nanosheets exhibits significantly cracked surfaces in the SEM image of g-$C_3N_4$-[HDBU]OH with average particle size of 9-12 nm. Although significant increase in the surface roughness is noted, the particle size does not change significantly from that of g-$C_3N_4$. $TiO_2$ displayed a spherical surface morphology with an increase in particle size from 22 nm to 102 nm for the SILP. [HDBU]OH can interact in various ways with different supports such as g-$C_3N_4$ and $TiO_2$ and allows for tailoring size of nanoparticles and surface morphology of the supports in SILP materials.

***Keywords***: Supported ionic liquid phase, Protic ionic liquid, DBU, Nanoparticle, Surface morphology

## I. Introduction

Ionic liquids (ILs) are widely recognized for their exceptional solubility, stability, and tunable properties and serve as unique media for the dispersion of nanoparticles (NPs) to improve mechanical, thermal, and electrical properties[1,2]. The incredibly low vapor pressure of ILs makes synthetic procedures possible at reduced pressure. ILs can serve better than organic solvents as media and catalysts for preparation and stabilization of nanoparticles and nanocomposites[3,4]. The supported ionic liquid phase (SILP) materials may be very efficient as an IL is able to reduce the diffusion distances of the reactants[5]. SILP materials help in resolving problems of limitations of mass transport and the need for large amounts of ILs by allowing ILs to spread on the inner surface of the supports while maintaining mechanical properties and wide surface area ILs can be immobilized as thin films on porous surfaces simply by chemically attaching to the support or by physisorption. ILs, whether interacted with or without chemical bonds, serve as a unique medium to integrate with homogeneous or heterogeneous catalysts[6]. Heterogeneous catalysis offers many more advantages including reduced catalyst loading, reusability, and ease of catalyst separation. In contrast, homogeneous catalytic processes necessitate a disproportionately large number of ILs as catalysts, resulting in waste that is difficult to dispose of and making the entire process environmentally unfriendly.

Hence, there has been a surge of interest on ILs in a number of significant heterogeneous catalytic processes. ILs with alkyl chain specifically functions as a capping agent to control shape of metal oxide NPs[7]. ILs with a range of transition metal NPs are capable of producing stable nanoparticle dispersions with enhanced catalytic activity. Materials chemistry has advanced two significant fields with extensive research of ILs on the one hand[8] and NPs on the other hand[9] in the last several decades. The many technical uses of NPs, especially in catalysis, are greatly influenced by their size, shape, and composition[10-11]. The concept of supported ionic liquid catalysis (SILC) has, thus, gained popularity due to the simplicity of the conversion process for bulky and complicated organic compounds[12]. The incorporation of ILs may often significantly increase the catalytic effectiveness of the NPs[13]. Their synergistic action allows SILP materials to derive a number of unique performances and novel properties while still retaining the benefits of ILs and NPs. Noble metal NPs, like gold and silver, are considered stronger supports on a variety of materials because of their distinct catalytic, electrical, and optical characteristics[14]. Carbon nanotubes (CNTs), zeolites, clays (such as montmorillonite), mesoporous silica materials, and metal/metal oxide NPs are the most common supports that bind

* Author for correspondence. e-mail: susan@du.ac.bd

ILs[15]. The ILs and supports can make covalent linkage when ILs with particular functional groups (OH-, R-O-R′, etc.) and pre-functionalized solid surfaces interact[16]. Sometimes, cations of the supported IL can act independently as catalysts. Metal-free functionalized ILs and sulfonic acid are used to prepare SILP materials. The SILP materials are superior to other catalysts in terms of mild conditions, rapid reaction time, and reusability.

Numerous investigations have reported preparation of hybrid NPs for use as supports for Brønsted acidic ILs[17]. The approach has significantly reduced acidic waste and demonstrated phenomenal competence in extraction of catalysts and recycling. Hydrophilic ILs facilitate interaction with NPs while hydrophobic ILs inhibit aggregation of NPs[18]. SILP materials exhibit efficient catalysis for oxidative degradation of organic compounds in presence of UV-visible light[19]. The nanocomposite materials based on g-$C_3N_4$ and $TiO_2$ are, in particular, reported as stable and efficient photocatalysts to facilitate the breakdown of organic molecules[20-21]. In this regard, ILs immobilized g-$C_3N_4$/$TiO_2$ composites have been effective with extended UV-visible light response[22-23]. There are many different approaches for oxidative degradation of organic compounds using NPs based catalysts, the majority of them have drawbacks, including the use of harmful and expensive chemicals, lengthy processes, extreme reaction conditions that only produce low or moderate yields, and inadequate catalysts in terms of recycling[24]. Therefore, development of novel SILP materials for better catalytic performance still remains an important concern.

Considering the advantageous features of ILs and usefulness of supported NPs, we aimed to develop new SILP materials using a protic ionic liquid, 1,8-diazabicyclo[5.4.0]undec-7-ene-8-ium hydroxide ([HDBU]OH) and graphitic carbon nitride (g-$C_3N_4$) and $TiO_2$ nanomaterials. To the best of our knowledge, the use of 1,8-diazabicyclo[5.4.0]undec-7-ene (DBU) based protic ILs has not been studied in the preparation of SILP materials. We report herein, preparation of g-$C_3N_4$-[HDBU]OH and $TiO_2$-[HDBU]OH by following a simple refluxing route. The goal is to modify the surface of the g-$C_3N_4$ and $TiO_2$ using [HDBU]OH which may have the potential to absorb UV-visible light and improve the breakdown of organic compounds in aqueous system. The formation of the novel SILP was traced from the FTIR and UV-visible absorption spectral analyses. The surface property and the size of the particle of the prepared SILP materials were evaluated from SEM images and DLS measurements. The ultimate goal is to explore the prospect of SILP materials for application as catalyst in degradation of organic compounds in presence of UV-visible light.

## II. Experimental

*Materials*

Analytical grade chemicals were used as received. 1,8-diazabicyclo[5.4.0]undec-7-ene from Sigma-Aldrich (China) and acetic acid from RCI Labscan Ltd. (Thailand) were used for the preparation of ILs. Melamine powder from Sigma-Aldrich and ethyl acetate from BDH Chemicals Ltd, England were used. Ultrapure water (specific conductivity is 0.055 μS $cm^{-1}$ at 25 °C) was prepared from a BOECO (Germany) HPLC-grade water purification system.

*Preparation of g-$C_3N_4$ and $TiO_2$ nanoparticles*

The g-$C_3N_4$ and $TiO_2$ nanoparticles were prepared following the procedure reported in the literature[25-26]. $TiO_2$ was prepared by heating a mixture of polyvinyl pyrrolidone (0.02 g), titanium tetra-isopropoxide (5 mL), absolute ethanol (30 mL) and deionized water (40 mL) to 130 °C for 12 h in an oven. Ammonia solution was added dropwise to maintain the pH of the reaction mixture 9. To prepare g-$C_3N_4$, melamine was heated to 450-550 °C at a rate of 3 °C per min for 7 h in autoclave.

*Preparation of [HDBU]OH*

[HDBU]OH was prepared by following the method (Scheme 1) reported earlier[27], where equal amount of water (6.569 mmol) and DBU (6.569 mmol) were added in a vial placed in an ice bath and sonicated for 30 min.

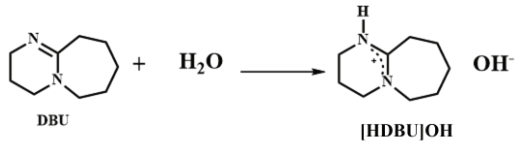


**Scheme 1.** Neutralization reaction of water and DBU.

*Preparation of g-$C_3N_4$-[HDBU]OH and $TiO_2$-[HDBU]OH*

In a round bottomed flask, 3 mmol of g-$C_3N_4$ or $TiO_2$ and 15 mL of ethyl acetate were taken and sonicated for 15 min. 3 mmol of [HDBU]OH was added dropwise and the mixture was refluxed for 4 h. It was then cooled down to room temperature. The product was separated by filtration, washed with DI water, and dried at 60 °C under vacuum. The preparation is schematically presented in Scheme 2.

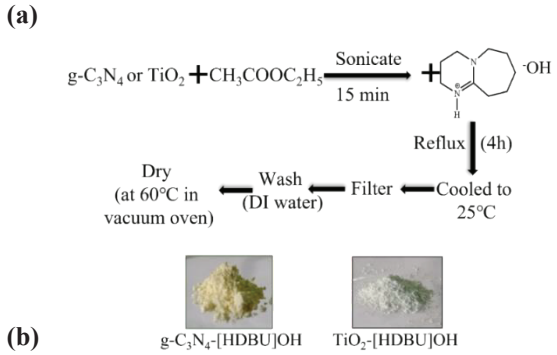


**Scheme 2.** (a) Schematic route for the preparation and (b) photographic images of g-$C_3N_4$-[HDBU]OH and $TiO_2$-[HDBU]OH.

*Characterizations*

FTIR spectra were recorded by a *Frontier*$^{TM}$ by PerkinElmer spectrophotometer with 20 scans for each sample in absorbance

mode in KBr. Gaussian profiles were created by deconvoluting and smoothing the raw spectra. Before performing deconvolution, each spectrum had baseline correction, and each peak fitting obtained an $R^2$ value of 0.9991.

Field emission scanning electron microscopic (FESEM) images were acquired by ZEISS Sigma 300, Germany, and Hitachi S3400N. The SEM images were captured applying accelerating potential of 5.00 kV at 150.00 KX magnification and 3.1–3.3 mm of Z-height.

A Zetasizer Nano ZS90 (ZEN3690, Malvern Instruments Ltd, UK) particle size analyzer was used to measure the diameters of the aggregates of nanoparticles and SILP materials using DLS measurements. The measurements were conducted at a fixed scattering angle of 90 degrees using a He-Ne laser beam with a wavelength of 632.8 nm. The hydrodynamic dimeter ($D_h$) of the particles present was determined by analyzing the scattering intensity data. A 10-mm-diameter measuring glass cell was employed. The detection limit of particle size was around 0.3 nm-5 µm. The accuracy of $D_h$ was ± 2%. The run time was set at 30 s for each sample and at least 3 measurements, each of 30 runs were carried out for each sample.

The UV-visible absorption spectra were recorded using a UV-1800, Shimadzu, Japan, single-beam UV-visible absorption spectrophotometer. The aqueous dispersions of g-$C_3N_4$, $TiO_2$, g-$C_3N_4$-[HDBU]OH, and $TiO_2$-[HDBU]OH were used for UV-visible absorption measurements.

## III. Results and Discussion

[HDBU]OH was prepared by neutralization reaction between DBU and water [27]. Using two supports g-$C_3N_4$ and $TiO_2$, two SILP materials, g-$C_3N_4$-[HDBU]OH, and $TiO_2$-[HDBU]OH have been prepared (Scheme 2) and characterized by FTIR, UV-visible spectral analyses, SEM images, and DLS measurements. The potential interactions in SILP materials that keep ILs immobilized on the solid surface of the support materials include chemical attachment and/or physical attraction. Through physisorption and/or chemical interactions, [HDBU]OH can be immobilized as thin films on porous surfaces of NPs. The presence of hydroxyl groups on the surface of the $TiO_2$ and the nature of surface charge of g-$C_3N_4$ can form hydrogen bonds, electrostatic or ion-dipole interactions with anions and cations of [HDBU]OH. The nanopores or mesopores of both $TiO_2$ and g-$C_3N_4$ allow capillary-condensing the [HDBU]OH that can help stronger physical immobilization. A good wetting behavior of [HDBU]OH can provide even spreading and film formation on the surface of NPs.

### *FTIR spectral analyses of g-$C_3N_4$ and g-$C_3N_4$-[HDBU]OH*

FTIR spectral analyses were carried out to determine structure of the prepared g-$C_3N_4$-[HDBU]OH (Fig. 1). The characteristic bands at 1323-1570 $cm^{-1}$ resemble the C-N bending mode of heterocycles, at 1635 $cm^{-1}$ for C=N stretching mode and at 806 $cm^{-1}$ for triazine units describe the structure of g-$C_3N_4$NPs (Fig. 1(a))[28]. In Fig. 1(b), the FTIR spectrum of g-$C_3N_4$-[HDBU]OH shows all characteristic bands for g-$C_3N_4$ along with a broad band in the wavenumber range of 3000-3500 $cm^{-1}$. The deconvolution of the broadband ($R^2$ = 0.9965) clearly shows the presence of N-H stretching mode at 3051, 3143, and 3200 $cm^{-1}$, confirming the existence of [HDBU]OH in g-$C_3N_4$-[HDBU]OH. The $OH^-$ stretching mode has been found in the region of 3300-3500 $cm^{-1}$.

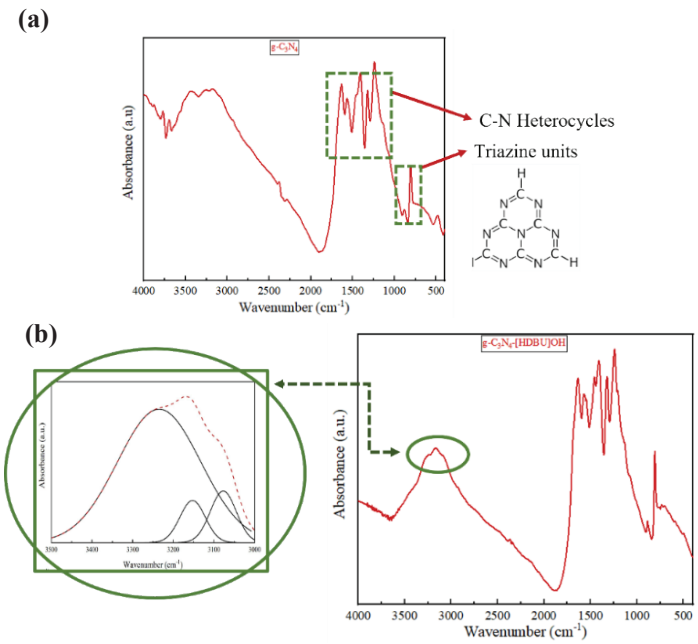


**Fig. 1.** FTIR spectra of **(a)** g-$C_3N_4$, and**(b)** g-$C_3N_4$-[HDBU]OH with deconvoluted spectra in the region of 3000-3500$^{-1}$ cm.

*FTIR spectral analyses of $TiO_2$ and $TiO_2$-[HDBU]OH*

Fig. 2 shows FTIR spectral analyses to determine the structure of the prepared $TiO_2$-[HDBU]OH. The characteristic band at 551 $cm^{-1}$ is for the Ti-O- stretching mode, at 1402 $cm^{-1}$ for Ti-O-Ti stretching, 1628 $cm^{-1}$ for OH- bending, and 3410 $cm^{-1}$ for OH- stretching describe the structure of $TiO_2$ NPs (Fig. 2(a))[29]. In Fig. 2(b), all characteristics bands for $TiO_2$ were present along with bands at 2854 and 2927 $cm^{-1}$ for C-H stretching bands in the region 900-1200 $cm^{-1}$ for appearance of C-N stretching and an overlapped broad band in the region of 3000-3500 $cm^{-1}$ indicates the presence of [HDBU]OH in $TiO_2$-[HDBU]OH. The broad band upon deconvolution ($R^2$= 0.9912) clearly shows the N-H stretching mode at 3076, 3154, and 3238 $cm^{-1}$, confirming the presence of [HDBU]OH in $TiO_2$-[HDBU]OH. The $OH^-$ stretching mode has been found in the region 3300-3500 $cm^{-1}$.

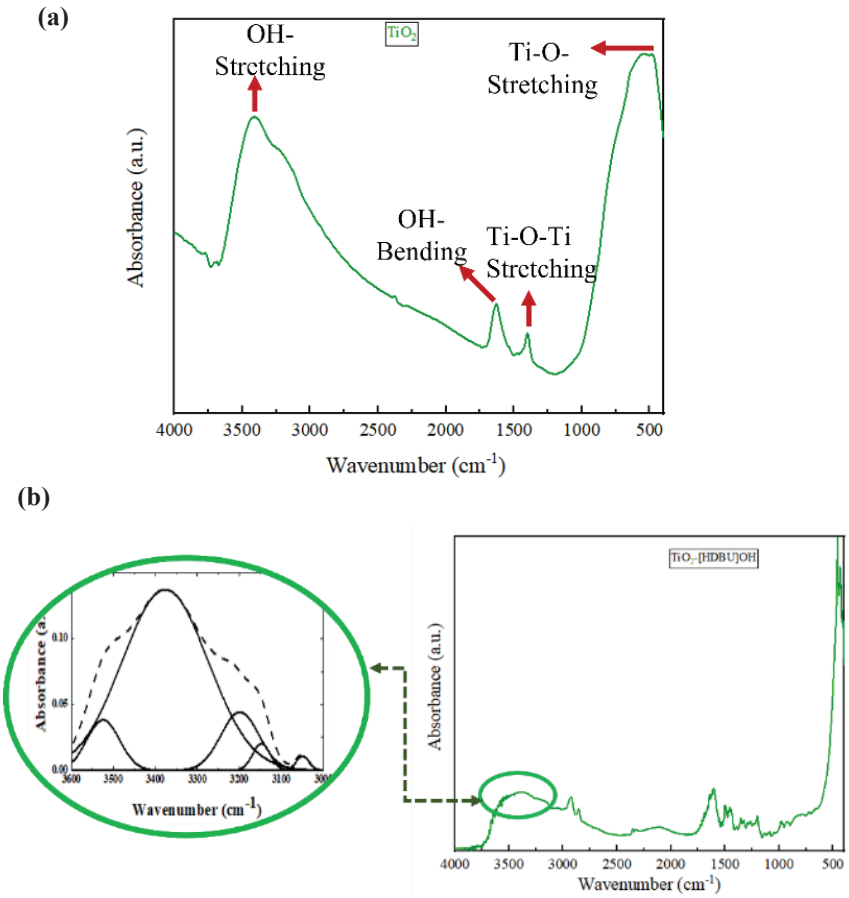


**Fig. 2.** FTIR spectra of **(a)** $TiO_2$, and **(b)** $TiO_2$-[HDBU]OH with deconvoluted spectra in the region of 3000-3500 $cm^{-1}$.

*UV-visible absorption spectral analyses of g-$C_3N_4$, $TiO_2$, g-$C_3N_4$ -[HDBU]OH, and $TiO_2$-[HDBU]OH in aqueous dispersion*

The UV-visible absorption spectra were investigated for g-$C_3N_4$, g-$C_3N_4$-[HDBU]OH, $TiO_2$, and $TiO_2$-[HDBU]OH in aqueous dispersion (Fig. 3). The absorption spectra for g-$C_3N_4$ and $TiO_2$ did not show characteristics absorption maxima. Same amount of material was taken to prepare the aqueous dispersion but the supernatant for $TiO_2$-[HDBU]OH showed very poor intensity as compared with that of g-$C_3N_4$-[HDBU]OH in the UV absorption spectra. The wavelength corresponding to absorption maximum was found for [HDBU]OH at 282 nm. Interestingly, the new SILP materials showed absorption maxima at different wavelengths from that of [HDBU]OH at 207, 327, and 392 nm for g-$C_3N_4$-[HDBU]OH and at 329, 296, 283, and 266 nm for $TiO_2$-[HDBU]OH.

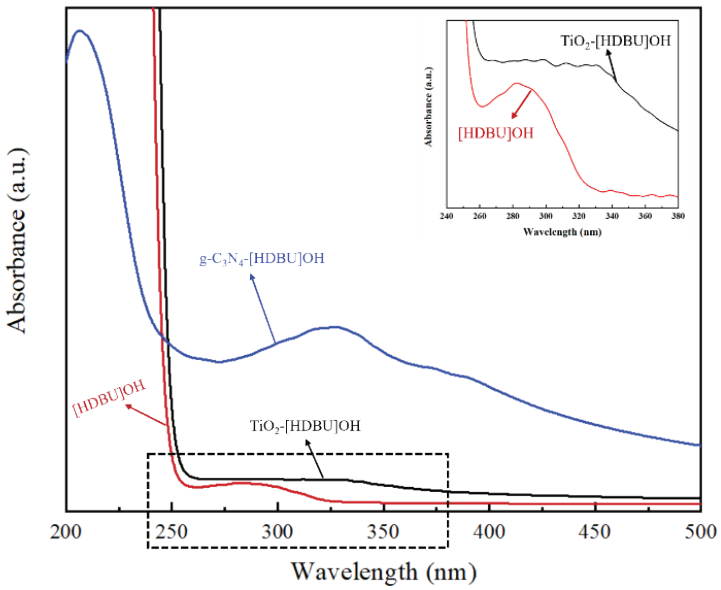


**Fig. 3.** UV-visible absorption spectra for aqueous dispersion of g-$C_3N_4$-[HDBU]OH, [HDBU]OH, and $TiO_2$-[HDBU]OH with an inset for the region of 240-380 nm (marked by dotted box).

*Surface morphology and particle size analyses of g-$C_3N_4$ and g-$C_3N_4$ -[HDBU]OH*

The individual particle shape and surface appearance of g-$C_3N_4$ and g-$C_3N_4$-[HDBU]OH have been investigated by SEM images (Fig. 4(a) and Fig. 4(b). The particles in g-$C_3N_4$ were uniformly distributed like a sheet with average size of the particles of 10-12 nm. The presence of [HDBU]OH over the g-$C_3N_4$ matrix is shown by the visible cracking of the nanosheets in g-$C_3N_4$-[HDBU]OH and resulting increased roughness with similar average size of the particles around 9-10 nm (Fig. 4(b)).

On the other hand, the study of particle size from DLS measurement of g-$C_3N_4$ and g-$C_3N_4$-[HDBU]OH is shown in Fig. 4(c) and 4(d), respectively. The $D_h$ includes the hydration layer around the particles in the suspension. The $D_h$ of around 80% particles in g-$C_3N_4$-[HDBU]OH is 132 nm and nearly the same as that of g-$C_3N_4$, which was 154 nm (Fig.4(c)). In g-$C_3N_4$-[HDBU]OH, only about 20% particles had an increased hydrodynamic diameter of 423 nm. The trend in the change in particle size from SEM measurements is consistent with that from DLS measurements (Fig. 4).

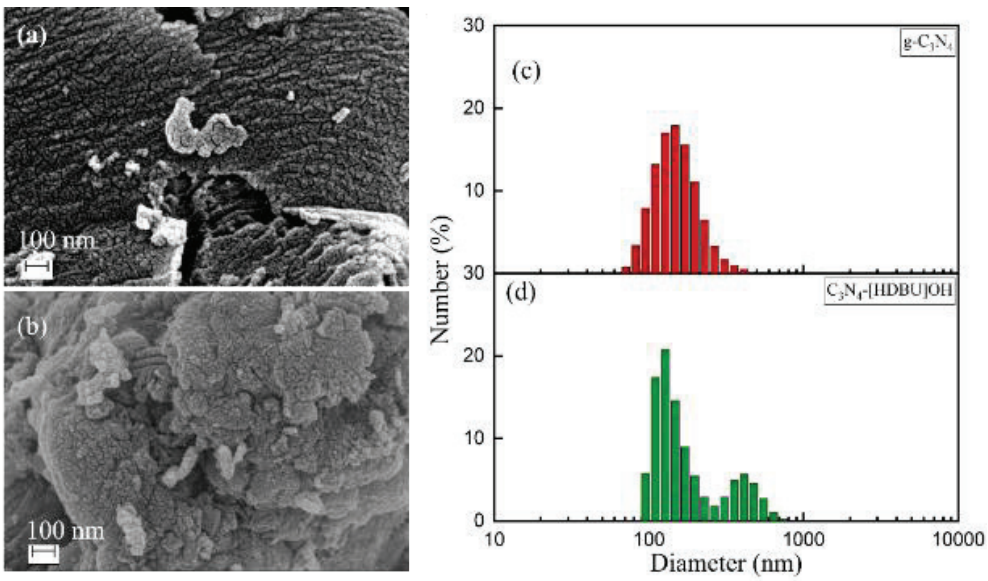


**Fig. 4.** SEM images of **(a)** g-$C_3N_4$ and **(b)** g-$C_3N_4$-[HDBU]OH and particle size distribution of **(c)** g-$C_3N_4$ and **(d)** g-$C_3N_4$-[HDBU]OH.

*Surface morphology and particle size analyses of $TiO_2$ and $TiO_2$-[HDBU]OH*

The SEM images of $TiO_2$ and $TiO_2$-[HDBU]OH have been investigated to show the individual particle shape and surface appearance and are shown in Fig. 4(a) and Fig. 4(b), respectively. Fig. 4(a) shows the surface morphology of spherical particles around 18-20 nm in $TiO_2$. The particle size increased up to 157 nm for $TiO_2$-[HDBU]OH to indicate that [HDBU]OH facilitated aggregation of $TiO_2$

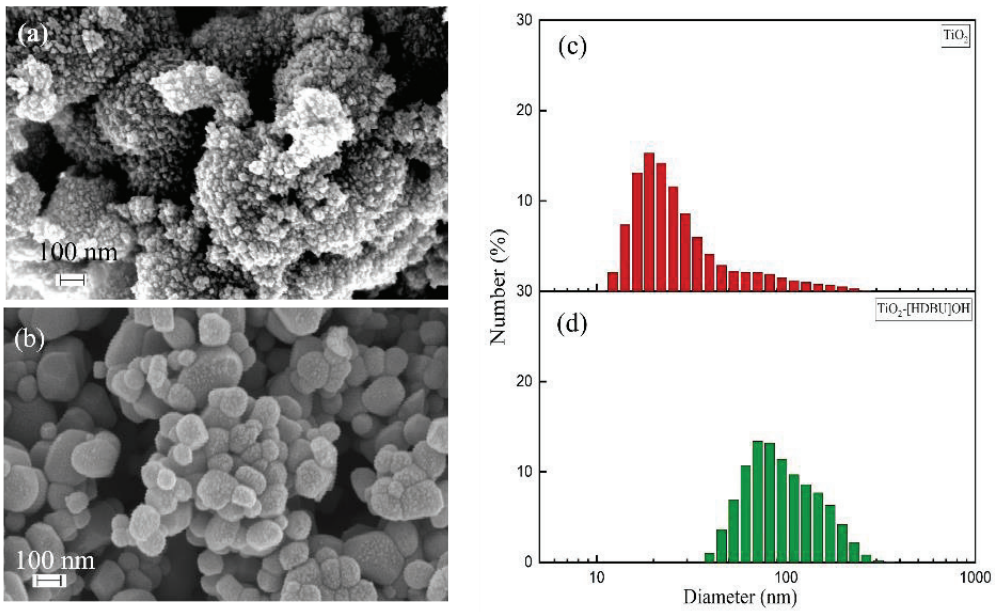


**Fig. 5.** SEM images of **(a)** $TiO_2$ and **(b)** $TiO_2$-[HDBU]OH and particle size distribution of **(c)** $TiO_2$ and **(d)** $TiO_2$-[HDBU]OH.

.

DLS measurements have been carried out to evaluate the $D_h$ of the particles in the suspension of $TiO_2$ and $TiO_2$-[HDBU]OH in water as shown in Fig. 5(c) and Fig. 5(d), respectively. The $D_h$ of $TiO_2$ is shown around 22 nm and increased to 102 nm in $TiO_2$-[HDBU]OH. A notable increase in particle size in $TiO_2$-[HDBU]OH suggests that [HDBU]OH plays an important role in the aggregation of $TiO_2$ particles. The variation of the particle size of $TiO_2$ and $TiO_2$-[HDBU]OH in their SEM images shows a similar trend to that of the DLS measurement (Fig. 5).

It was reported that IL could prevent association of nanoparticles and collapse of pore structure of solid support materials, that helps increase in surface area. A few investigations reported usage of some imidazolium based aprotic ILs in modifying nanoparticles as photocatalysts with improved photoactivity[30]. The photocatalytic activity of IL-NP varies with variation of the nature anions of ILs[31]. Therefore, different ILs can modify the size NPs in different ways. Thus, the g-$C_3N_4$-[HDBU]OH could show improved photocatalytic activity with increased surface area. On the other hand, $TiO_2$-[HDBU]OH could exhibit reduced photocatalytic performance with increased size (decreased surface area) of the particles.

[HDBU]OH has the potential to tune the size of the particles of support materials, g-$C_3N_4$ and $TiO_2$ in the SILP materials. In g-$C_3N_4$-[HDBU]OH, about 80% particles have the particle size similar to the g-$C_3N_4$ NPs. Thus, it is expected that the SILP materials would retain the catalytic activity of g-$C_3N_4$ in presence of UV light identical. Significant cracking on the surface of g-$C_3N_4$ was observed in g-$C_3N_4$-[HDBU]OH. The SILP, g-$C_3N_4$-[HDBU]OH, may provide increased surface area of the particles because of the enhanced roughness on the surface of g-$C_3N_4$ and could show increased catalytic activity. On the other hand, $TiO_2$-[HDBU]OH, showed a significant increase from 22 nm to 102 nm in particle size, indicating that [HDBU]OH improved the capacity of the $TiO_2$ to aggregate. Hence, [HDBU]OH when immobilized on the surface of g-$C_3N_4$ and $TiO_2$ can tune the size of the particles of the supports in SILP materials. The PIL, [HDBU]OH is also able to tailor the surface morphology in g-$C_3N_4$-[HDBU]OH by inducing cracks on the surface and in $TiO_2$-[HDBU]OH by increasing the combining capacity of the particles.

$TiO_2$ and g-$C_3N_4$ are generally used as catalysts in heterogeneous photocatalysis due to many unique properties including potent oxidation and reduction capabilities, and high chemical stability. However, the applications are limited by low activity in the visible area of the solar spectrum and the slow rate of electron transfer to oxygen while excited electron-hole pairs recombine. To comprehend the mechanism of excitation of IL-NP materials, it is crucial to investigate how the structure of ILs affects the surface characteristics and activity due to visible light. Imidazolium-based aprotic ILs have been used successfully in a

few studies to modify the surface of the NPs as photocatalysts with enhanced photoactivity. Thus, attempt may be made to regulate the band gap, surface area, charge separation efficiency, and visible light absorption capacity of NPs using the potential of DBU based PILs in the SILP materials. Oxygen vacancies in $TiO_2$ and nitrogen vacancies in g-$C_3N_4$ may be created due to interaction with ILs and may promote effective charge separation while retaining a substantial level of oxidation capacity.

## IV. Conclusions

[HDBU]OH can be used to prepare two new supported ionic liquid phase materials, g-$C_3N_4$-[HDBU]OH and $TiO_2$-[HDBU]OH using a simple refluxing method. The g-$C_3N_4$ may show the catalytic activity, as the prepared g-$C_3N_4$-[HDBU]OH showed negligible increase in the size of only 20% particles. Moreover, the SILP, g-$C_3N_4$-[HDBU]OH is expected to improve the overall catalytic performance of g-$C_3N_4$ because of the insignificant agglomeration of the particles and enhanced roughness on the surface of the support material. A notable increase in particle size from 22 nm to 102 nm in $TiO_2$-[HDBU]OH suggests that [HDBU]OH assisted the tendency of $TiO_2$ to aggregate. [HDBU]OH can modify g-$C_3N_4$ and $TiO_2$ in different ways, and it can contribute significantly to the improve performances and surface morphological characteristics in g-$C_3N_4$-[HDBU]OH and $TiO_2$-[HDBU]OH.

## Acknowledgement

GA acknowledges the financial support of the University Grants Commission (UGC) Bangladesh through Postdoctoral Fellowship 2023. The authors also acknowledge Jashore University of Science and Technology (JUST) for providing access to the FESEM measurements facilities.

## References

1. Hirano, M., K. Enokida, K. I. Okazaki, S. Kuwabata, H. Yoshida, and T. Torimoto, 2013. Composition-dependent electrocatalytic activity of AuPd alloy nanoparticles prepared via simultaneous sputter deposition into an ionic liquid. *Physical Chemistry Chemical Physics*, ***15***, 7286-7294.
2. Wasserscheid, P. and T. Welton, 2008. Ionic liquids in synthesis, vol. 1, Weinheim: Wiley-VCH.
3. Armand, M., F. Endres, D. R. MacFarlane, H. Ohno, and B. Scrosati, 2009. Ionic-liquid materials for the electrochemical challenges of the future. *Nature Materials*, ***8***, *621-629*.
4. Al-Salman, R., X. Meng, J. Zhao, Y. Li, U. Kynast, M. M. Lezhnina, and F. Endres, 2010. Semiconductor nanostructures via electrodeposition from ionic liquids. *Pure and Applied Chemistry*, ***82***, 1673-1689.
5. Lemus, J., J. Palomar, M. A. Gilarranz, and J. J. Rodriguez, 2011. Characterization of supported ionic liquid phase (SILP) materials prepared from different supports. *Adsorption*, ***17***, 561-571.
6. Li, H., P. S. Bhadury, B. Song, and S. Yang, 2012. Immobilized functional ionic liquids: efficient, green, and reusable catalysts. *RSC Advances*, ***2***, 12525-12551.
7. Husanu, E., V. Cappello, C. S. Pomelli, J. David, M. Gemmi, and C. Chiappe, 2017. Chiral ionic liquid assisted synthesis of some metal oxides. *RSC Advances*, *7*, 1154-1160.
8. Zhang, Q., S. Zhang, and Y. Deng, 2011. Recent advances in ionic liquid catalysis. *Green Chemistry*, ***13***, 2619-2637.
9. Gawande, M. B., A. K. Rathi, P. S. Branco, and R.S. Varma, 2013. Sustainable utility of magnetically recyclable nano-catalysts in water: applications in organic synthesis. *Applied Sciences*, ***3***, 656-674.
10. Raoof, J. B., S. R. Hosseini, and S. Rezaee, 2015. A simple and effective route for preparation of platinum nanoparticle and its application for electrocatalytic oxidation of methanol and formaldehyde. *Journal of Molecular Liquids*, ***212***, 767-774.
11. Ghosh, S., S. S. Acharyya, D. Tripathi, and R. Bal, 2014. Preparation of silver–tungsten nanostructure materials for selective oxidation of toluene to benzaldehyde with hydrogen peroxide. *Journal of Materials Chemistry A*, ***2***, 15726-15733.
12. Candu, N., C. Rizescu, I. Podolean, M. Tudorache, V. I. Parvulescu, and S. M. Coman, 2015. Efficient magnetic and recyclable SBILC (supported basic ionic liquid catalyst)-based heterogeneous organocatalysts for the asymmetric epoxidation of trans-methylcinnamate. *Catalysis Science & Technology*, ***5***, 729-737.
13. Wang, D., and Y. Li, 2011. Bimetallic nanocrystals: liquid-phase synthesis and catalytic applications. *Advanced Materials*, ***23***, 1044-1060.
14. Kamat, P. V., 2002. Photophysical, photochemical and photocatalytic aspects of metal nanoparticles. *The Journal of Physical Chemistry B*, ***106***, 7729-7744.
15. Welton, T., 2008. Is catalysis in ionic liquids a potentially green technology. *Green Chemistry*, ***10***, 483-483.
16. Bhuyan, B., B. Paul, S. Vadivel, and S. S. Dhar, 2016. Preparation and characterization of $WO_3$ bonded imidazolium sulfonic acid chloride as a novel and green ionic liquid catalyst for the synthesis of adipic acid. *RSC Advances*, ***6***, 99044-99052.
17. Xin, B. and J. Hao, 2014. Imidazolium-based ionic liquids grafted on solid surfaces. *Chemical Society Reviews*, ***43***, 7171-7187.

18. Gandhi, R. R., S. Gowri, J. Suresh, and M. Sundrarajan, 2013. Ionic liquids assisted synthesis of ZnO nanostructures: controlled size, morphology and antibacterial properties. *Journal of Materials Science and Technology*, ***29***, 533-538.

19. Chakraborty, D., M. Devi, B. Das, M. H. Barbhuiya, S. S. Dhar, and A. Chowdhury, 2021. A benevolent direction to environmental suitability: ionic liquid immobilized $MoO_3$ nanoparticles used in the efficient visible light-driven photocatalytic degradation of antibiotics. *New Journal of Chemistry*, ***45***, 12922-12930.

20. He, X., Z. Wu, Y. Xue, Z. Gao, and X. Yang, 2019. Fabrication of interlayer β-CD/g-$C_3N_4$@ $MoS_2$ for highly enhanced photodegradation of glyphosate under simulated sunlight irradiation. *RSC Advances*, ***9***, 4635-4643.

21. Bayan, E. M., L. E. Pustovaya, and M. G. Volkova, 2021. Recent advances in $TiO_2$-based materials for photocatalytic degradation of antibiotics in aqueous systems. *Environmental Technology & Innovation*, ***24***, 101822.

22. Raziq, F., M. Humayun, A. Ali, T. Wang, A. Khan, Q. Fu, W. Luo, H. Zeng, Z. Zheng, B. Khan, and H. Shen, 2018. Synthesis of S-Doped porous g-$C_3N_4$ by using ionic liquids and subsequently coupled with Au-$TiO_2$ for exceptional cocatalyst-free visible-light catalytic activities. *Applied Catalysis B: Environmental*, ***237***, 1082-1090.

23. Nayebi, M., A. Faraji, A. Bahadoran, Z. J. Othman, S. Arghavani, P. G. Kargar, S. M. Sajjadinezhad, and R. S. Varma, 2023. $TiO_2$/g-$C_3N_4$/$SO_3H$ (IL): unique usage of ionic liquid-based sulfonic acid as an efficient photocatalyst for visible-light-driven preparation of 5-HMF from cellulose and glucose. *ACS Applied Materials & Interfaces*, ***15***, 8054-8065.

24. Dai, J., W. Zhong, W. Yi, M. Liu, L. Mao, Q. Xu, and D. Yin, 2016. Bifunctional $H_2WO_4$/TS-1 catalysts for direct conversion of cyclohexane to adipic acid: Active sites and reaction steps. *Applied Catalysis B: Environmental*, ***192***, 325-341.

25. Yan, S. C., Z. S. Li, and Z. G. Zou, 2009. Photodegradation performance of g-$C_3N_4$ fabricated by directly heating melamine. *Langmuir*, ***25***, 10397-10401.

26. Wiranwetchayan, O., S. Promnopas, T. Thongtem, A. Chaipanich, and S. Thongtem, 2017. Effect of alcohol solvents on $TiO_2$ films prepared by sol–gel method. *Surface and Coatings Technology*, ***326***, 310-315.

27. Ara, G., M. S. Miran, M. M. Islam, M. Y. A. Mollah, M. M. Rahman, M. A. B. H. Susan, 2020. 1, 8-Diazabicyclo [5.4. 0]-undec-7-ene based protic ionic liquids and their binary systems with molecular solvents catalyzed Michael addition reaction. *New Journal of Chemistry*, ***44***, 13701-13706.

28. Tan, L., J. Xu, X. Zhang, Z. Hang, Y. Jia, and S. Wang, 2015. Synthesis of g-$C_3N_4$/$CeO_2$ nanocomposites with improved catalytic activity on the thermal decomposition of ammonium perchlorate. *Applied Surface Science*, ***356***, 447-453.

29. Vetrivel, V., K. Rajendran, and V. Kalaiselvi, 2015. Synthesis and characterization of pure titanium dioxide nanoparticles by sol-gel method. *International Journal of ChemTech Research*, ***7***, 1090-1097.

30. Jing, L., M. Wang, X. Li, R. Xiao, Y. Zhao, Y. Zhang, Y. M. Yan, Q. Wu, and K. Sun, 2015. Covalently functionalized $TiO_2$ with ionic liquid: A high-performance catalyst for photoelectrochemical water oxidation. *Applied Catalysis B: Environmental*, ***166***, 270-276.

31. Łuczak, J., M. Paszkiewicz-Gawron, M. Długokęcka, W. Lisowski, E. Grabowska, S. Makurat, J. Rak, and A. Zaleska-Medynska, 2017. Visible-Light Photocatalytic Activity of Ionic Liquid $TiO_2$ Spheres: Effect of the Ionic Liquid's Anion Structure. *ChemCatChem*, ***9***, 4377-4388.